

Stoichiometry determination of chalcogenide superlattices by means of X-ray diffraction and its limits

Felix Rolf Lutz Lange and Matthias Wuttig

*I. Physikalisches Institut (IA), RWTH Aachen University, 52056 Aachen, Germany and
JARA-FIT Institute Green-IT, RWTH Aachen University and Forschungszentrum Jülich, 52056 Aachen, Germany*

Henning Hollermann, Stefan Jakobs, and Peter Kernes

*I. Physikalisches Institut (IA), RWTH Aachen University, 52056 Aachen, Germany
(Dated: December 14, 2024)*

In this paper we explore the potential of stoichiometry determination for chalcogenide superlattices via X-ray diffraction. To this end, a set of epitaxial GeTe/Sb₂Te₃ superlattice samples with varying layer thicknesses is sputter-deposited. Kinematic scattering theory is employed to link the average composition with the diffraction features. The observed lattice constants of the superlattice reference unit cell follow Vegard's law, enabling a straight-forward stoichiometry determination.

I. INTRODUCTION

GeTe/Sb₂Te₃ chalcogenide superlattices (CSL, also referred to as interfacial phase change memory (iPCM)) have attracted significant interest for next generation data storage. This interest arises from enhanced switching speeds, improved endurance as well as reduced power consumption compared to conventional PCRAMs.¹ Beyond their application relevance, these superlattices (SLs) possess fascinating physical properties, such as topologically protected surface states,^{2,3} which renders CSLs interesting also for fundamental research. Indeed, superlattices in general are a very active area of research and SL-based applications like e.g. solid-state lasers⁴ or thermoelectrics⁵ have become an integral part of modern technology. The key to reliable and predictable material and device performance, however, is based on a precise control of the SLs structure. A thorough structural characterization is thus mandatory to develop successful growth recipes and benchmark the quality of the SL structure. Compared with doped semiconductors and alloys, SLs provide an additional level of complexity. While the stoichiometry of an alloy can be characterized by a single parameter, a SL requires two additional parameters to be defined precisely, namely the layer thicknesses of the two constituting materials (cf. Fig. 1(b)). Owing to this complexity, SLs span a huge parameter space to alter physical properties via tuning knobs such as the average composition of the SL, its bilayer thickness and the resulting interface density as well as the number of repetitions. In the case of CSLs, the structural characterization mainly rests on studies using (scanning) transmission electron microscopy in conjunction with energy-dispersive X-ray spectroscopy ((S)TEM/EDX) as well as X-ray diffraction (XRD) methods. The combination of TEM and EDX is powerful to access all structural parameters on a single lamella. Studies utilizing these two techniques have already provided important information on the local atomic arrangement at GeTe/Sb₂Te₃ interfaces.^{6,7} Yet, TEM suffers from time-consuming sample preparation and destructivity. XRD

on the other hand does not face these drawbacks, but provides non-local structural information without the need of any prior preparation. Nevertheless, it is mainly used to verify the SL character by the observation of peaks of larger intensity, that are surrounded by satellite peaks whose spacing can be translated to the unit cell size of the superlattice.^{8,9} In the present work we show that the analysis of these characteristic features can be used to determine the stoichiometry of any given CSL. To this end, we utilize kinematic scattering theory to derive the average composition of the CSL. The model utilized will be shown to be equivalent to a description in terms of Vegard's law¹⁰ which assumes a linear relationship between the lattice size and the composition of alloy crystals. For SL structures, however, such a linear dependence is not obvious since both parent materials are subject to stress and strain. Thus an elastic response obeying the elastic constants of the parent materials is conceivable. In fact, literature provides examples of both cases, systems following^{11–13} and systems incompatible with^{14–17} Vegard's law. In the case of III-V SLs, Vegard's law is frequently employed to estimate the stoichiometry of the SL,^{18–20} while for systems like CdTe/ZnTe,¹⁷ PbTe/EuTe¹⁴ and TiAlN/CrN¹⁶ deviations are reported. In the case of SLs which incorporate V₂IV₃ compounds such as Sb₂Te₃ the situation is potentially even more complex as these materials are composed of van-der-Waals-like gaps featuring a weak coupling of adjacent building blocks.^{21,22} Hence, the applicability of Vegard's law for stoichiometry determination is not guaranteed. Here, we will validate the model for SLs of GeTe and Sb₂Te₃ as this pair of materials at present forms the most promising combination when it comes to iPCM applications. Finally, the limits of the method are explored and possible error sources identified.

II. STOICHIOMETRY DEPENDENCE OF DIFFRACTION DATA

A superlattice, as a repeated epitaxial stacking of two (or more) materials, is described by its own unique unit cell, called supercell. The out-of-plane periodicity of the SL is given by the sum of the thicknesses of the parent materials and is referred to as the bilayer thickness Λ . Therefore the set of possible diffraction maxima is $Q_z^{(n')} = 4\pi \frac{\sin \Theta}{\lambda} = n' \frac{2\pi}{\Lambda}$. Fig. 1 shows the XRD pattern of such a superlattice. All diffraction peaks can be explained as integer multiples of the primitive reciprocal lattice $2\pi/\Lambda$, directly related to the bilayer thickness. Fig. 1(a) shows the peak positions extracted from XRD data for several such superlattice samples with different Λ plotted against the peak index n' . From the slope of the linear fit the supercell size can be determined. Yet, it is striking that for this system only a few evenly spaced diffraction peaks of significantly varying intensity are observed. This pattern, which appears unconventional at first sight, needs a convincing explanation.

There are three possible explanations for the small number of diffraction peaks observed. a) There could be a high number of generic defects such as a multitude of grain boundaries in the film causing broadening of all diffraction peaks. Instead a distinctive pattern is observed, where only certain peaks are observed. b) Hence, there could be *one characteristic* defect, characterized by a distinctive vector, such as a Burgers vector for a certain dislocation type. In this case, a characteristic extinction pattern is expected, with systematic intensity annihilations that can be described as a multiples of a characteristic reciprocal vector. Again, this incompatible with the observation of a pattern characterized by a regular appearance rather than a disappearance of peaks. c) The third remaining possibility becomes evident upon comparison to similar samples grown by molecular beam epitaxy (MBE) or when sputtering them on muscovite mica substrates. Such films, which can be produced with higher crystal quality, show groups of peaks over slightly wider regions of reciprocal space. This implies that film imperfections cause a significant number of diffraction peaks to vanish. From TEM it is known that in a CSL not only one single supercell size is favored, but various GeTe and Sb₂Te₃ layer thicknesses coexist within the CSL stack.²³ During deposition variations by one or more fundamental building blocks of our constituents - namely Te-Sb-Te-Sb-Te blocks, the quintuple layers (QTs) of Sb₂Te₃ and Ge-Te blocks, the bilayers (BLs) of GeTe - are highly likely. Since XRD is an averaging technique, it obtains intensity from a large set of such slightly differently stacked grains. Hence, only peak groups around the mean lattice periodicity persist. Away from these regions in reciprocal space, the lattices with different supercell size dephase, lowering the scattering intensity (cf. suppl. material). However, the relative peak intensities within each peak group show a pronounced intensity asymmetry, which must be governed

by the structure factor of the SL. Since this structure factor depends on the positions of the atoms within the supercell, it contains information on the stoichiometry of the superlattice. This is confirmed by the data shown in Fig. 2, where diffraction patterns of three SL samples with similar Λ but different composition are displayed together with Sb₂Te₃ and GeTe reference samples. Clearly, the positions of the intense peaks change with stoichiometry. On the other hand, the intensity distribution of all samples displayed in Fig. 1 is comparable, even though the size of the superlattice cell differs significantly, since they share the same stoichiometry.

Nevertheless, the direction of the shift of the positions of the peak groups with composition shown in Fig. 2 seems surprising at first sight. From Vegard's law we would expect that a change to more Sb₂Te₃-rich SLs and thus the substitution of some Ge by the larger Sb atoms, would lead to an increase in mean lattice spacing, defined by the mean distance of the common Tellurium sublattice of both constituents. This should shift all peak groups to smaller Q_z values. However, we observe the opposite, which can be explained by the different structures of GeTe and Sb₂Te₃. GeTe consists of stacked Ge-Te bilayers (BLs), while the Sb₂Te₃ unit cell consists of three QTs that are coupled across van-der-Waals-like gaps^{21,23}. As a consequence, the Te-Te layer distance at the van-der Waals like gaps is shorter than the Te-Te layer distance within the QT. Therefore, the mean Te-Te distance between adjacent layers is smaller in Sb₂Te₃ ($d_{\text{Sb}_2\text{Te}_3}^{(0009)} \approx 3.38 \text{ \AA}$) than in GeTe ($d_{\text{GeTe}}^{(0003)} \approx 3.53 \text{ \AA}$) (c.f. Fig. 1(b)). From Fig. 2, the characteristic distance of peak groups is determined to $\Delta Q_z \approx 1.82 \text{ \AA}^{-1}$, which translates to a plane spacing of about 3.45 \AA . The distance corresponds to the average Te-Te layer spacing in the corresponding sample²⁴. A change in chemical composition of the SL sample can therefore be observed by XRD. The peaks observed are referred to in the literature as superlattice peaks (highlighted in orange in Fig. 2) which are flanked by a number of satellite peaks (lighter orange). As explained above, this naming scheme is a convenient description only all peaks belong to the same family of planes of the supercell. However, these labels stem from the reference lattice concept,^{25,26} which is often employed to describe the diffraction pattern of multi-layer structures.^{9,11,27} We will now show how the concept can be used to deduce the chemical composition of any given SL from XRD-data. In a pseudomorphic superlattice, the supercell size Λ is composed of a discrete number of lattice planes of the parent materials

$$\Lambda = n_1 d_1 + n_2 d_2 \quad (1)$$

with d_1 and d_2 being lattice plane spacings of the constituent materials. For the SL discussed here the plane distances $d_{\text{GeTe}}^{(0003)}$ and $d_{\text{Sb}_2\text{Te}_3}^{(0009)}$ correspond to the mean Te-Te layer distances in either material and consequently n_1 and n_2 are the number of those Te layers (c.f. Fig. 1(b)). To complete the reference lattice description

we use Eq. (1) to define a fraction \bar{d} of the supercell as the mean plane spacing (Te-Te layer spacing)

$$\bar{d} := \frac{\Lambda}{n_1 + n_2} \quad (2)$$

The diffraction peaks in terms of the reference lattice are therefore indexed by a modified Braggs law as^{9,26}

$$Q_z^{(n')} = n' \frac{2\pi}{\Lambda} \Leftrightarrow Q_z^{(m,n)} = m \cdot \frac{2\pi}{\bar{d}} \pm n \cdot \frac{2\pi}{\Lambda} \quad (3)$$

with $m, n = 0, 1, 2, \dots$ and $n' = m(n_1 + n_2) + n$. Peaks labeled by m are the superlattice peaks belonging to the reference lattice and peaks indexed by n are the superlattice satellites (c.f. Fig. 2). Since the stoichiometry determination relies on the difference in lattice plane distances between d_1 and d_2 , the average Te-Te layer spacing \bar{d} can be used to determine the compositional ratio $\eta = n_2/n_1$ of the constituent materials as follows

$$\bar{d} = \frac{d_1 + \eta d_2}{1 + \eta}. \quad (4)$$

It may be noted that the absolute values of \bar{d} and η depend on the choice of d_1 and d_2 that describe the supercell (c.f. Eq. (1)). If Eqs. (3) and (4) are combined the compositional ratio of a SL can be obtained from a diffraction experiment as

$$\eta = \frac{d_1 - 2\pi/\Delta Q_z}{2\pi/\Delta Q_z - d_2}, \quad (5)$$

where $\Delta Q_z = Q_z^{(m+1,0)} - Q_z^{(m,0)}$ is the distance of two subsequent SL peaks. Furthermore, if we write Eq. (4) in the form

$$\bar{d} = d_1(1 - x_2) + x_2 d_2, \quad (6)$$

where $x_2 = n_2/(n_1 + n_2) = \eta/(\eta + 1)$, it becomes evident that \bar{d} scales monotonously and linearly with the amount of either constituent material, resembling Vegard's law for alloys as described above. Therefore, a successful description in terms of Eq. (5) will verify the applicability of Vegard's law. In the following, after giving information about the methods used, we will present and discuss the experimental results on the stoichiometry dependence of \bar{d} .

III. METHODS

To validate the model a series of GeTe/Sb₂Te₃ SLs are sputter deposited from stoichiometric targets with a purity of 99.99 at.% on Si(111)-H substrates at deposition temperatures ranging from 180°C to 210°C. By variation of the deposition times used for both materials, the thicknesses $t_{\text{Sb}_2\text{Te}_3}$ and t_{GeTe} are varied. The average plane spacing \bar{d} is obtained for each sample by X-ray diffraction using a Bruker D8 Discover setup equipped

with a Goebel mirror and a two-bounce Ge(220) ACC monochromator. The compositional ratio η is measured by energy-dispersive X-ray spectroscopy with an FEI Helios 650 NanoLab system (electron beam: 10 keV, 0.4 nA, scan-area: 200 μm × 300 μm) and the Oxford Instruments AZtec software (version 2.1) for data recording and analysis. Additional information on sample characterization is detailed in the supplementary information.

IV. RESULTS

The lattice mismatch of the constituent materials amounts to 2.5% for the (0001) orientation. As it has been demonstrated in previous work,⁷ for this growth direction and elevated temperatures we expect quasi-vander-Waals epitaxy of the two materials and thus the formation of a CSL. As motivated above, our SL samples are conveniently described by a reference lattice with $\bar{d} \approx 3.45 \text{ \AA}$, defined by the plane distances $d_1 = d_{\text{GeTe}}^{(0003)}$ and $d_2 = d_{\text{Sb}_2\text{Te}_3}^{(0009)}$ in Eq. (1) (c.f. Fig. 1(b)). Hence we index the SL peaks in Fig. 2 as (0 0 m). In the limit of Vegard's law, also the in-plane lattice constant a can be expressed similarly to Eq. (4) as

$$a = \frac{a_{\text{GeTe}} + \eta a_{\text{Sb}_2\text{Te}_3}}{1 + \eta}, \quad (7)$$

In order to experimentally test Eqs. (4) and (7), a set of plane families has been measured by XRD, namely {0001}, {11̄21}, {11̄22} and {11̄23}. Their peak center was determined by subsequent φ , ψ , ω , Θ and $2\Theta/\omega$ measurements in bisecting geometry. The a - and \bar{d} -axes were subsequently obtained by a least-square algorithm. Using this method, the relative errors on a and c are in the range of 0.3% and 0.5%, respectively. In addition, the c -axis was also determined by Θ - 2Θ scans (along Q_z) for a larger set of samples. Here, a linear regression of $Q_z^{(m,0)}$ with diffraction order m was used to obtain \bar{d} . The corresponding EDX data was analyzed assuming a stoichiometric $(\text{GeTe})_x(\text{Sb}_2\text{Te}_3)_{1-x}$ SL. All three combinations of ratios (Ge/Sb, Ge/Te and Sb/Te) were used to calculate η . The final value is a weighted average with an estimated EDX resolution of 1 at.%. Fig. 3 shows the result of this investigation. As can be seen, Eqs. (4) and (7) (dashed-dotted lines) nicely reproduce the experimental data. The change in unit cell thus follows Vegard's law. The model was fitted with a_{GeTe} and $a_{\text{Sb}_2\text{Te}_3}$ or c_{GeTe} and $c_{\text{Sb}_2\text{Te}_3}$ as free parameters, respectively. Their values $a_{\text{Sb}_2\text{Te}_3} = 4.275 \text{ \AA}$, $c_{\text{Sb}_2\text{Te}_3} = 9 \cdot d_{\text{Sb}_2\text{Te}_3}^{(0009)} = 30.591 \text{ \AA}$, $a_{\text{GeTe}} = 4.177 \text{ \AA}$ and $c_{\text{GeTe}} = 3 \cdot d_{\text{GeTe}}^{(0003)} = 10.606 \text{ \AA}$ agree well with data reported in literature for bulk samples $a_{\text{Sb}_2\text{Te}_3} = 4.264 \text{ \AA}$, $c_{\text{Sb}_2\text{Te}_3} = 30.459 \text{ \AA}$,²⁸ $a_{\text{GeTe}} = 4.156 \text{ \AA}$ and $c_{\text{GeTe}} = 10.663 \text{ \AA}$.²⁹ Therefore the model can be used to estimate the stoichiometry by obtaining either the lattice parameter a or \bar{d} of the reference lattice and use Eqs. (5) to calculate η . It should be noted, that with

knowledge of η and Λ (obtained from the SL peak position and the satellite spacing) also the layer thicknesses t_{GeTe} and $t_{\text{Sb}_2\text{Te}_3}$ of the parent materials can be deduced that comprise Λ .

V. DISCUSSION

The last part of this paper illuminates potential error sources and estimates the error of this method depending on a) the stoichiometry factor η , b) the bilayer thickness Λ , and c) the interface density $\rho_{\text{int}} \sim \Lambda^{-1}$. From Fig. 3 it is apparent, that the stoichiometry can be deduced with highest accuracy in the proximity of $\eta = 1$, where the slope of $\bar{d}(\eta)$ is steepest. In case of $\eta \rightarrow 0$ and $\eta \rightarrow \infty$, the lattice constants approach the values of GeTe and Sb_2Te_3 layers, respectively. Here, large changes in η will amount in subtle changes of \bar{d} , causing large errors on the stoichiometry. In literature, working CSL devices have been demonstrated with values of η ranging from $3 \leq \eta \leq 7.5$.^{1,30-32} Within this stoichiometry window, the relative error on η is estimated to be of the order of 10% with $Q_z^{(m,0)}$ of accuracy of 0.5% or better³³ (see supplementary information). Eqs. (5) and (6) are based on a precise determination of the peak center of the SL reference peaks. This becomes challenging if the bilayer thickness Λ becomes large enough for the peak areas of the zeroth order Bragg peak and its satellites to overlap. In this case, a proper deconvolution of peaks is mandatory to obtain $Q_z^{(m,0)}$. Assuming a full-width at half-maximum of $\beta = 0.015 \text{ \AA}^{-1}$ of the SL peaks and satellites, the maximum bilayer thickness without significant overlap is estimated to be $\Lambda_{\text{max}} = \frac{2\pi}{2\beta} = 209 \text{ \AA}$. This value amounts to roughly four times the bilayer thickness reported by Simpson et al.¹ for successful device operation ($\Lambda \approx 47 \text{ \AA}$). Yet, this estimation relies on the structural quality of the CSL as β broadens with the defect density, the vertical coherence length and stress/strain in the system.

As shown by Momand et al.,^{6,7,23} CSLs deposited at elevated temperatures tend to intermix at the interfaces, thus forming building blocks of thermodynamically stable $(\text{GeTe})_x(\text{Sb}_2\text{Te}_3)_{1-x}$ alloys (GST). This adds further complexity to Eq. (1) since in principle a third plane spacing d_{GST} would have to be considered. As this intermixing is most pronounced at the interface, its impact is expected to scale with the interface density $\rho = \Lambda^{-1}$. To

investigate the impact of the intermixing on the model, several CSL have been sputter deposited with the same compositional ratio η , but varying bilayer thicknesses Λ ranging from 20 to 140 \AA . Fig. 4 shows the result of this investigation. As can be seen, for high interface densities (small values of Λ) the \bar{d} -axis of the reference lattice deviates from the proposed value given by Eq. (4) (dashed-dotted line in Fig. 4). The maximum deviation, however, only amounts to 0.5%, thus proving the model still a good estimate, even for high interface densities. For these high-interface densities we assume that due to intermixing the CSL structure dissolves into the stable rhombohedral GST structure which – unlike the meta-stable cubic phase³⁴ – also follows Vegard’s law as reported by Karpinsky et al.³⁵ Their data points are also displayed in Fig. 3 (green squares). The systematic deviation is most likely caused from the difference between bulk samples (Karpinsky et al.) and thin-films (this study). Using first-principle calculations, the experimental values were corroborated by Da Silva et al. for both, the a and c axes of bulk GST.³⁶ Interestingly, the authors also understand the GST structure as a superlattice-like-stacking of Sb_2Te_3 and GeTe. Clearly, a CSL unit cell made of a single GeTe bilayer intercalated into Sb_2Te_3 quintuples results in a stable GST structure. To verify this generic behavior, a GeSb_2Te_4 thin-film was sputter-deposited at 300°C from a stoichiometric target. As can be seen in Fig. 3 (red triangle), also this sample is nicely described by the model presented above. In summary, the limits of stoichiometry determination via X-ray diffraction for $\text{GeTe}/\text{Sb}_2\text{Te}_3$ superlattices have been explored. The measured change in lattice constants obeys Vegard’s law. This insight can be used to estimate the stoichiometry of any SL by a straight-forward evaluation of diffraction peaks. Intermixing at the $\text{GeTe}/\text{Sb}_2\text{Te}_3$ interface does not affect the reference unit cell noticeably. This method thus provides a fast alternative to TEM/EDX for stoichiometry determination even for CSL structures in complex device structures. The results obtained here can be extended to related SLs systems composed of (IV-VI):(V₂VI₂) materials or other p-bonded chalcogenides.

ACKNOWLEDGMENTS

The financial support by the DFG through SFB 917 is gratefully acknowledged. This work was also partially funded by the PASTRY project (GA 317746) within the FP7 of the EU.

¹ R. E. Simpson, P. Fons, A. V. Kolobov, T. Fukaya, M. Krabal, T. Yagi, and J. Tominaga, *Nature Nanotechnology* **6**, 501 (2011).

² B. Sa, J. Zhou, Z. Sun, J. Tominaga, and R. Ahuja, *Physical Review Letters* **109**, 096802 (2012).

³ J. Tominaga, A. V. Kolobov, P. Fons, T. Nakano, and

S. Murakami, *Advanced Materials Interfaces* **1** (2014), 10.1002/admi.201300027.

⁴ S. Nakamura, M. Senoh, S.-i. Nagahama, N. Iwasa, T. Yamada, T. Matsushita, H. Kiyoku, and Y. Sugimoto, *Applied Physics Letters* **68**, 3269 (1996).

⁵ M. S. Dresselhaus, G. Chen, M. Y. Tang, R. G. Yang,

H. Lee, D. Z. Wang, Z. F. Ren, J.-P. Fleurial, and P. Gogna, *Advanced Materials* **19**, 1043 (2007).

⁶ J. Momand, R. Wang, J. E. Boschker, M. A. Verheijen, R. Calarco, and B. J. Kooi, *Nanoscale* **7**, 19136 (2015).

⁷ J. Momand, F. R. L. Lange, R. Wang, Jos E. Boschker, M. A. Verheijen, R. Calarco, M. Wuttig, and B. J. Kooi, *Journal of Materials Research* **31**, 3115 (2016).

⁸ V. S. Speriosu and T. Vreeland, *Journal of Applied Physics* **56**, 1591 (1984).

⁹ E. E. Fullerton, I. K. Schuller, H. Vanderstraeten, and Y. Bruynserae, *Physical Review B* **45**, 9292 (1992).

¹⁰ L. Vegard, *Zeitschrift für Physik* **5**, 17 (1921).

¹¹ A. Madan, P. Yashar, M. Shinn, and S. A. Barnett, *Thin Solid Films* **302**, 147 (1997).

¹² K. Brunner, K. Eberl, W. Winter, and E. Bugiel, *Applied Surface Science Proceedings of the International Symposium on Si Heterostructures: From Physics to Devices*, **102**, 17 (1996).

¹³ Y.-C. Liang and Y.-C. Liang, *Journal of Crystal Growth* **296**, 104 (2006).

¹⁴ A. Ishida, S. Matsuura, H. Fujiyasu, H. Ebe, and K. Shinozaki, *Superlattices and Microstructures* **2**, 575 (1986).

¹⁵ A. Y. Nikulin, A. W. Stevenson, and H. Hashizume, *Physical Review B* **53**, 8277 (1996).

¹⁶ D. B. Lewis, I. Wadsworth, W. D. Münz, R. Kuzel, and V. Valvoda, *Surface and Coatings Technology* **116**, 284 (1999).

¹⁷ G. Monfroy, S. Sivananthan, X. Chu, J. P. Faurie, R. D. Knox, and J. L. Staudenmann, *Applied Physics Letters* **49**, 152 (1986).

¹⁸ R. M. Blefeld, G. C. Osbourn, P. L. Gourley, and I. J. Fritz, *Journal of Electronic Materials* **12**, 903 (1983).

¹⁹ M. C. Joncour, M. N. Charasse, and J. Burgeat, *Journal of Applied Physics* **58**, 3373 (1985).

²⁰ H. Ng, C. Gmachl, S. Chu, and A. Cho, *Journal of Crystal Growth* **220**, 432 (2000).

²¹ R. Wang, F. R. L. Lange, S. Cecchi, M. Hanke, M. Wuttig, and R. Calarco, *Advanced Functional Materials* **28**, 1705901 (2018).

²² P. A. Vermeulen, J. Mulder, J. Momand, and B. J. Kooi, *Nanoscale* **10**, 1474 (2018).

²³ J. Momand, R. Wang, J. E. Boschker, M. A. Verheijen, R. Calarco, and B. J. Kooi, *Nanoscale* **9**, 8774 (2017).

²⁴ R. Wang, V. Bragaglia, J. E. Boschker, and R. Calarco, *Crystal Growth & Design* **16**, 3596 (2016).

²⁵ V. Holý, U. Pietsch, and T. Baumbach, *High-Resolution X-Ray Scattering from Thin Films and Multilayers*, Springer Tracts in Modern Physics, Vol. 149 (Springer Berlin Heidelberg, Berlin, Heidelberg, 1999).

²⁶ U. Pietsch, V. Holý, and T. Baumbach, *High-Resolution X-Ray Scattering: From Thin Films to Lateral Nanostructures* (Springer Science & Business Media, 2004).

²⁷ M. R. Khan, C. S. L. Chun, G. P. Felcher, M. Grimsditch, A. Kueny, C. M. Falco, and I. K. Schuller, *Physical Review B* **27**, 7186 (1983).

²⁸ T. L. Anderson and H. B. Krause, *Acta Crystallographica Section B: Structural Crystallography and Crystal Chemistry* **30**, 1307 (1974).

²⁹ P. Bauer, S. Gorsse, I. Sergueev, J. Dadda, E. Mueller, and R. Hermann, *physica status solidi (b)* **250** (2013), 10.1002/pssb.201248412.

³⁰ T. Ohyanagi, M. Kitamura, M. Araida, S. Kato, N. Takaura, and K. Shiraishi, *Applied Physics Letters* **104**, 252106 (2014).

³¹ T. Shintani and T. Saiki, *Applied Physics Express* **6**, 111401 (2013).

³² M. Tai, T. Ohyanagi, M. Kinoshita, T. Morikawa, K. Akita, S. Kato, H. Shirakawa, M. Araida, K. Shiraishi, and N. Takaura, in *2014 Symposium on VLSI Technology (VLSI-Technology): Digest of Technical Papers* (2014) pp. 1–2.

³³ M. A. Moram and M. E. Vickers, *Reports on Progress in Physics* **72**, 036502 (2009).

³⁴ T. Matsunaga, R. Kojima, N. Yamada, K. Kifune, Y. Kubota, Y. Tabata, and M. Takata, *Inorganic Chemistry* **45**, 2235 (2006).

³⁵ O. G. Karpinsky, L. E. Shelimova, M. A. Kretova, and J. P. Fleurial, *Journal of Alloys and Compounds* **268**, 112 (1998).

³⁶ J. L. F. Da Silva, A. Walsh, and H. Lee, *Physical Review B* **78**, 224111 (2008).

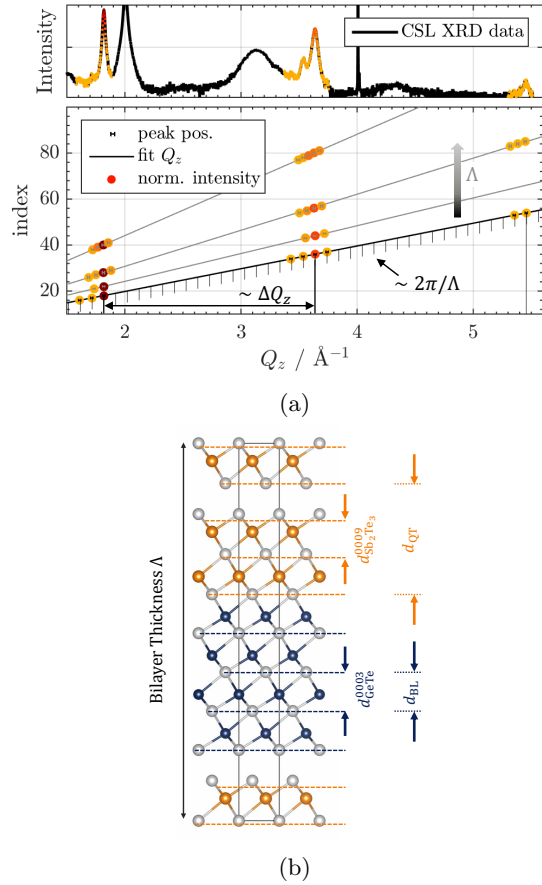


FIG. 1. (a) In the upper panel a typical diffraction pattern of a superlattice is shown. It is apparent that only a small number of closely spaced diffraction peaks stemming from the SL supercell are observed. This is due to the variation of supercell size that happens for all CSL samples during deposition. In the lower panel the positions of these superlattice peaks are plotted for a number of superlattices against the peak index, showing that each set of peaks belongs to one single plane family, namely the respective supercell. The different samples feature different supercell sizes, but they share the same composition. All four superlattices show the strongest diffraction peaks at similar positions in reciprocal space (red points). Their spacing translates to the mean Te-Te layer distance in the superlattice (reference lattice), which is a direct measure for composition. The asymmetric distribution of intensity within each peak group can also be attributed to the underlying structure factor of the supercell. (b) Depicted is an exemplary structural representation of a SL supercell as an epitaxial stacking of GeTe bilayers (BLs) and Sb₂Te₃ quintuple layers (QTs) projected along [001]. Also given are $d_{\text{Sb}_2\text{Te}_3}^{(0009)}$ and $d_{\text{GeTe}}^{(0003)}$ – the mean Te layer distances of either material. Note that in the case of Sb₂Te₃, we have van-der-Waals like gaps and therefore the (0009)-planes do not coincide with atom positions.

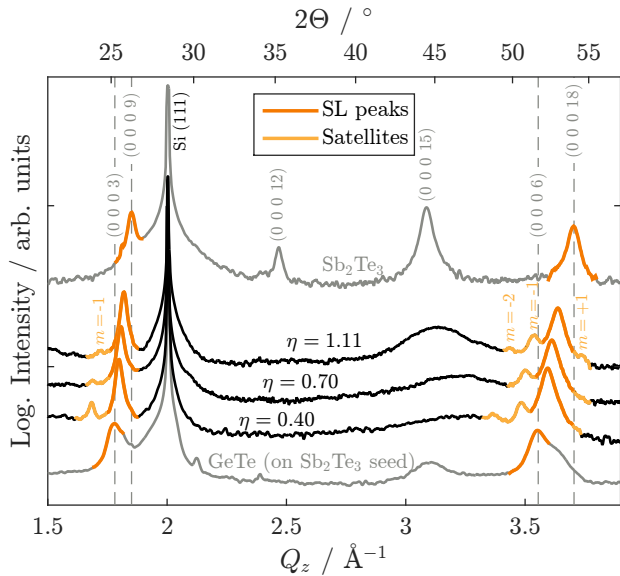


FIG. 2. Overview of diffraction patterns for GeTe/Sb₂Te₃ superlattices of similar supercell size Λ but different stoichiometry together with GeTe and Sb₂Te₃ reference samples. The peaks of the superlattice appear as groups around the mean Te-Te layer distance, which are labeled within the reference lattice description as superlattice peaks (orange) and neighboring satellites (lighter orange). With increasing stoichiometry ratio and therefore a shift to more Sb₂Te₃-rich SLs, the peak groups shift to larger Q_z , since the mean Te-Te distance decreases. This can be used to determine the stoichiometry from diffraction data.

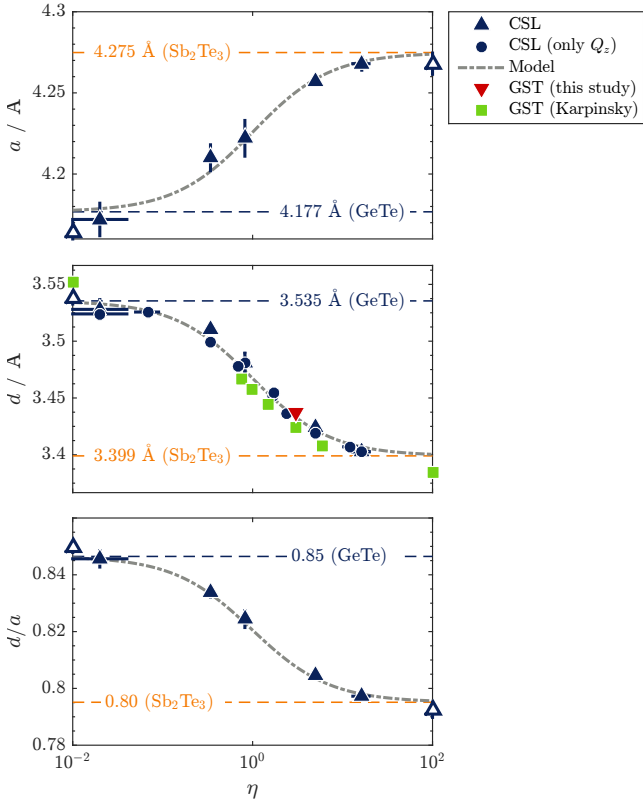


FIG. 3. Evolution of the SL reference lattice unit cell with composition. The data can be found in the supplemental material. Both parameters, \bar{d} and a follow 4 and (7), thus obeying Vegard's law. Moreover, it is found that CSLs follow the same generic behavior as their related $(\text{GeTe})_x(\text{Sb}_2\text{Te}_3)_{1-x}$ alloys (GSTs). The corresponding values for bulk samples are taken from Karpinsky et al.³⁵ The GST film (red triangle) refers to a GeSb_2Te_4 thin-film, deposited at 300C. Open markers at $\eta = 0.01$ and $\eta = 100$ refer to the two limiting cases of GeTe and Sb_2Te_3 realized by sputter-deposited thin-films of GeTe and Sb_2Te_3 , respectively.

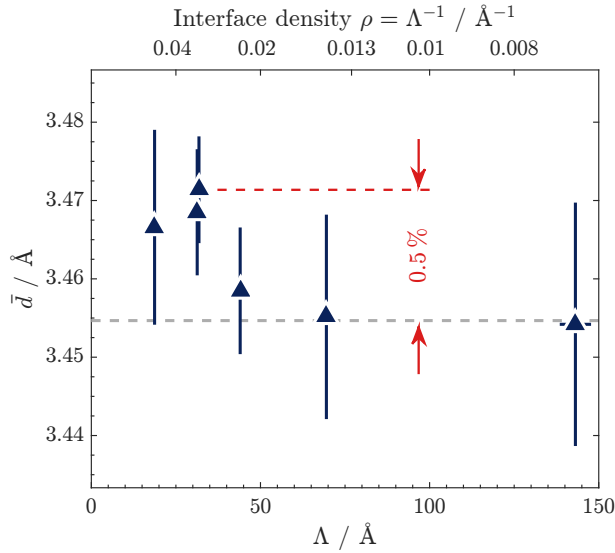


FIG. 4. Change of reference length \bar{d} with interface density ρ . Here, the compositional ratio is kept constant ($\eta = 1.8 \pm 0.1$). \bar{d} increasingly deviates from Eq. (4) when approaching large interface densities (smaller values of Λ). The overall discrepancy, however, is less than 0.5%, thus rendering \bar{d} still a good measure.